Electro-thermal Simulations of Nanoscale Transistors with Optical and Acoustic Phonon Heat Conduction

Jung-Hoon Chun, Bokyung Kim, Yang Liu, Olof Tornblad, and Robert W. Dutton
Center for Integrated Systems, Stanford University, CA 94305
E-mail: jhchun@gloworm.stanford.edu

***Abstract* -** **In order to take into account the nanoscale heat generation and phonon heat conduction, the optical and acoustic phonon temperature system for TCAD simulation is developed and self-consistently coupled with the hydrodynamic transport model. This electro-thermal model is validated through the simulations of a thin-body SOI NMOSFET.**

I. INTRODUCTION

As modern silicon transistors are continuously scaled down, the gate length becomes shorter than the mean free path of phonons. The small *hotspot* occupies a considerable portion of the carrier channel, therefore the electrical conductance can be seriously influenced by thermal characteristics [1].
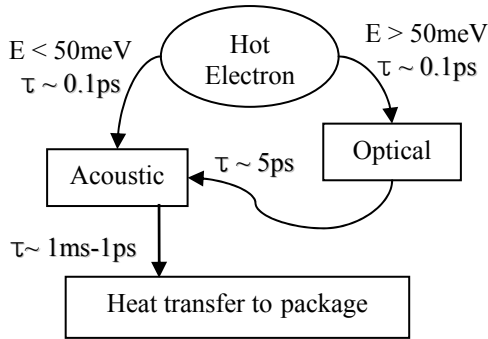

FIGURE 1: Energy transfer process diagram in silicon [1]. Electrons with high energy (> 50meV) effectively interact with optical phonons (τ~0.1ps), and then optical phonons decay into the acoustic modes (τ~5.0ps).

Heat generation and transport in the *hotspot* involve the coupling of electrons and various modes of phonons [1]. As illustrated in Fig. 1, high energy electrons (E > ~50 meV) scatter most effectively with optical phonons, however these phonons are relatively stationary. Therefore heat transport is mostly governed by acoustic phonons with large group velocity. The energy relaxation time between hot electrons and optical phonons is ~0.1 ps, while the relaxation time between optical phonons and acoustic phonons is ~5 ps. This relaxation time difference results in the energy accumulation in optical phonons; the accumulated energy is highly localized due to the small group velocity of optical phonons. Heat generation and conduction mechanisms with the multi-mode phonon dispersion have been thoroughly analyzed via Monte Carlo method [2]. However, this thermal analysis system still needs to be self-consistently coupled with electrical system and should be simplified for the simulations of complete transistor structures.

Another critical thermal phenomenon is the phonon boundary scattering at interfaces. The phonon boundary scattering seriously impedes heat transport in thin semiconductor devices such as ultra thin body SOI devices, FinFETs, and nanowires [3]. In order to take into account this phenomenon, the thermal conductivity of thin silicon films was carefully measured [4], and Tornblad. et al. [5] proposed an anisotropic thermal conductance model extracted from a linearized form of the Boltzmann transport equation.

In order to investigate the impact of the nanoscale thermal phenomena described above, a thermal system with optical and acoustic phonon temperatures was implemented, using the PDE based device simulator *PROPHET* [6]. This thermal system is concurrently coupled to the hydrodynamic carrier transport model. The details of the hydrodynamic model implemented in *PROPHET* can be found in [7]. The anisotropic thermal conductance model is also employed to investigate the impact of phonon boundary scattering in thin film devices. We performed simulations with SOI NMOSFET devices with 40 nm gate length and 20 nm SOI thickness.

II . GOVERNING EQUATIONS AND DEVICE INFORMATION

The heat transport equation can be written with the carrier temperature (T_c) and lattice temperature (T_l).

$$C_l \frac{\partial T_l}{\partial t} = \frac{3}{2} n \cdot k_B \cdot \frac{T_c - T_l}{\tau} + \nabla \cdot (\kappa \nabla T_l) \qquad (eq.1)$$

Where, C_l is the heat capacity of the lattice. k_B is the Boltzmann constant and κ is the lattice thermal conductivity. The first term in the right side is the energy transfer from the carriers (electrons or holes) to the lattice and τ is the carrier energy relaxation time. With this equation, the hydrodynamic carrier transport model can be coupled to the heat transport models. However, Eq.1 still cannot deal with the multi-mode energy transfer due to the phonon dispersion illustrated in Fig. 1.

In this work, the equations for energy transfer between carriers and phonons are implemented with two phonon temperatures (T_o for optical phonons and T_a for acoustic phonons) as follows,

$$C_o \frac{\partial T_o}{\partial t} = H + \nabla \cdot (\kappa_o \nabla T_o) - C_o \frac{T_o - T_a}{\tau_o} \qquad (eq.2)$$

$$C_a \frac{\partial T_a}{\partial t} = \nabla \cdot (\kappa_a \nabla T_a) + C_o \frac{T_o - T_a}{\tau_o} \qquad (eq.3)$$

Where, *Co (Ca)* is the heat capacity of the optical (acoustic) phonons. τ_o is the relaxation time for optical phonons

(~5.0ps). κ_a is the lattice thermal conductivity relevant to the propagating velocity of acoustic phonons, and κ_o is an adjustable parameter for the heat conduction through optical phonons. κ_o is much smaller than κ_a, since optical phonons are almost stationary. H is the energy transfer from electrons (or holes) to the optical phonons. H is almost same as the first term in the right side of Eq.1, but it should be rewritten in terms of T_o [8].

$$H = \frac{3}{2} n \cdot k_B \cdot \frac{T_c - T_o}{\tau} \qquad (eq.4)$$

This term can be replaced by a simple Joule heating, $J \cdot E$ (J is the current density and E is the electric field) in simulations with the drift-diffusion models.

In this work, we performed two-dimensional device simulations with various combinations of the electrical and thermal models; 1) the hydrodynamic model with Eq.2~4 ('two phonon temperature model'), 2) hydrodynamic model with Eq.1 ('one lattice temperature model'), and 3) drift-diffusion model with Eq.2~3, and $J \cdot E$ for the heat generation.
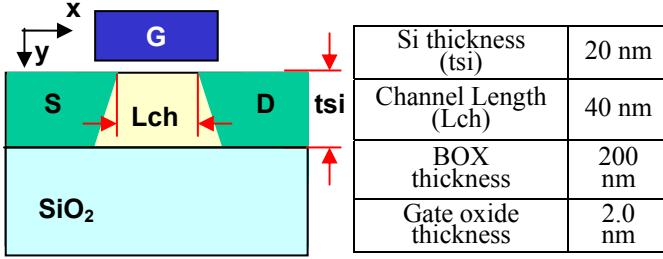

FIGURE 2: The geometric information of the simulated device, thin body SOI NMOSFET.

Si thickness (tsi)	20 nm	
Channel Length (Lch)	40 nm	
BOX thickness	200 nm	
Gate oxide thickness	2.0 nm	

In order to investigate the impact of the optical and acoustic phonon systems, a thin body SOI MOSFET based on [9] is employed for the simulations. The geometric information of the device is listed in Fig. 2. The effective channel length and silicon film thickness are 40 nm and 20 nm, respectively.
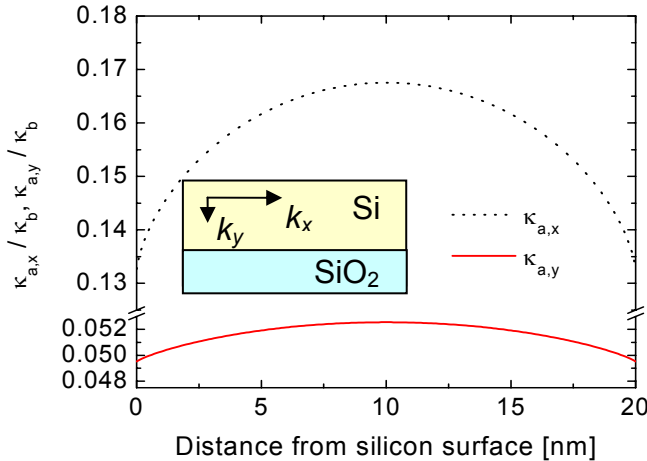

FIGURE 3: The anisotropic thermal conductivity in the 20 nm silicon film of the SOI NMOSFET in Fig. 2, normalized by the thermal conductivity at bulk silicon.

In Eq.2 and 3, κ_a is modeled as an anisotropic thermal

conductivity as follows [5],

$$\kappa_{a,x}(or\ \kappa_{a,y}) = \kappa_b \cdot \left(1 - \frac{1}{2}e^{-(\frac{y}{a \cdot \Lambda})^b} - \frac{1}{2}e^{-(\frac{D-y}{a \cdot \Lambda})^b}\right)$$

Here, Λ is the mean-free-path of acoustic phonons. D is the thickness of films. κ_b is the thermal conductivity at bulk silicon. (a, b) is (0.35, 0.75) for $\kappa_{a,x}$, and (0.72, 0.95) for $\kappa_{a,y}$. y is the position with reference to one edge of the thin silicon film. As shown in Fig. 3, the calculated anisotropic thermal conductivity in the 20 nm silicon film of the SOI NMOSFET is reduced to 5~17% of that of bulk silicon.

In order to predict electrical characteristics at high temperature, temperature dependency of the low-field mobility and electron saturation velocity models are modified according to [10, 11]. The mobility model strongly depends on the carrier temperature as in [7]. For setting proper thermal boundary conditions, source, drain, gate and substrate contacts are terminated with the finite thermal resistance.

III . SIMULATION RESULTS AND DISCUSSIONS

Fig. 4 shows the electron energy along the channel at the silicon/gate oxide interface. The gate bias is set to 1 V, and the drain bias varies from 0.2 V to 1.0 V with 0.2 V steps. At drain bias higher than 0.4 V, ~75% of the channel is occupied with electrons of >50 meV, which means the energy relaxation from electrons to phonons is dominated by the interaction between electrons and optical phonons.
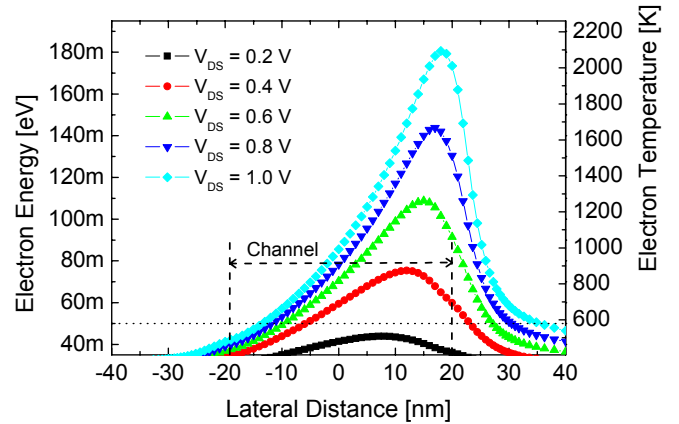

FIGURE 4: The electron energy along the channel at the silicon/gate oxide interface. V_{GS} is 1.0 V, and V_{DS} is 0.2 V~1.0 V. The physical channel is also indicated.

For comparing with 'the two phonon temperature model,' we also performed the simulation using just 'one lattice temperature model' (the hydrodynamic model with eq.1). Fig. 5 shows the simulated Id-Vd curves. With V_{GS} of 0.5 V and 0.75 V, there is no noticeable change in I-V characteristics between two models. However, in the high current and voltage regime, we can see a reduction of the current driving capability. Drain current decreases by ~5 % at $(V_{GS}, V_{DS}) = (1V, 1V)$. This reduction can be explained by the temperature profiles shown in Fig.6~8. Fig.6 shows the optical and acoustic phonon temperature profiles along the channel at the silicon/gate oxide interface. The lattice

temperature profile extracted from the simulation with the 'one lattice temperature model' is also plotted. Because the energy relaxation time between hot electrons and optical phonons is much shorter than the relaxation time between optical phonons and acoustic phonons, the energy is accumulated in optical phonons. So, the optical phonon temperature is considerably raised over the acoustic phonon temperature throughout almost half of the channel, and has its peak inside the drain region. When V_{GS} and V_{DS} are 1 V, the peak of the optical phonon temperature is ~455 K, and the peak of the acoustic phonon temperature is ~415 K. The lattice temperature profile extracted from simulations with 'one lattice temperature model' is almost the same as the acoustic temperature profile. Due to the higher optical phonon temperature and increased rate of scattering, the electron mobility (and saturation velocity) is degraded, resulting in the reduced drain current in Fig. 5.
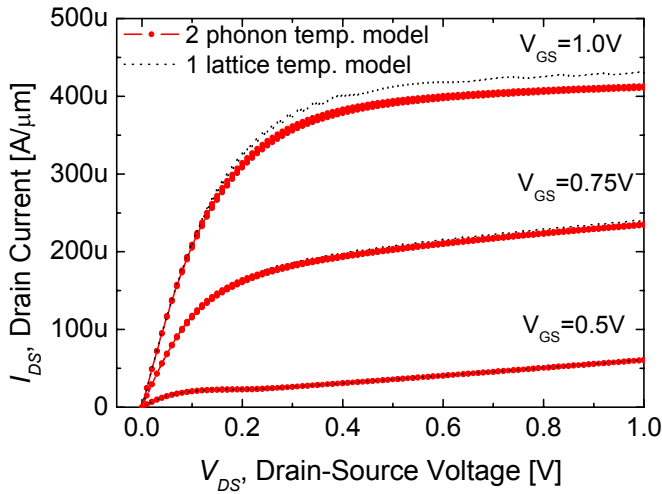
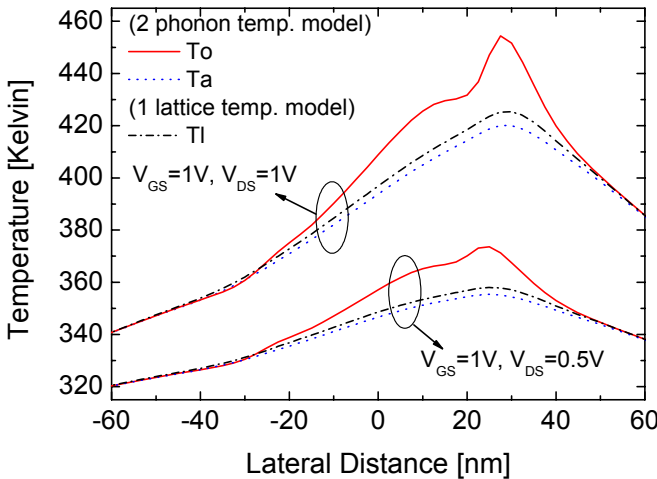FIGURE 5: Simulated I_D vs. V_{DS} curves with various gate biases.

FIGURE 6: Optical (*To*) and acoustic (*Ta*) phonon temperature along the channel at the silicon/gate oxide interface. Lattice temperature (*Tl*) extracted from the simulation with 'one temperature model' is also plotted.

Fig. 7 and 8 are two-dimensional contour plots for the optical and acoustic phonon temperatures. In each plot, the interval between contours is 10 Kelvin. It is clearly shown

that the generated heat is confined mostly inside the silicon film since the thermal conductivity is dramatically reduced due to the phonon boundary scattering. The hotspot of the optical phonons is severely localized because of the low group velocity of the optical phonons, while the generated heat is transferred to the contacts mainly by the acoustic phonons.
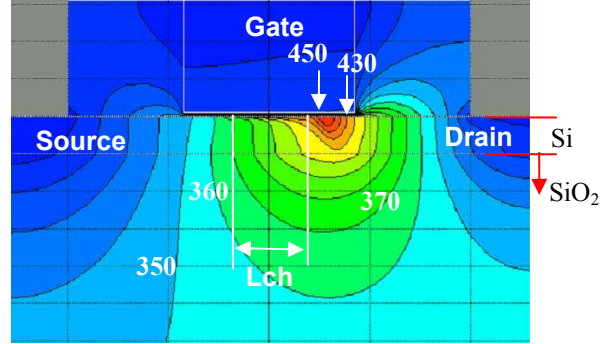
FIGURE 7: Two-dimensional contour plot of the optical phonon temperature. The interval between contours is 10 Kelvin. $V_{GS} = V_{DS} = 1$ V and $I_{DS} = $ ~0.4 mA/µm.
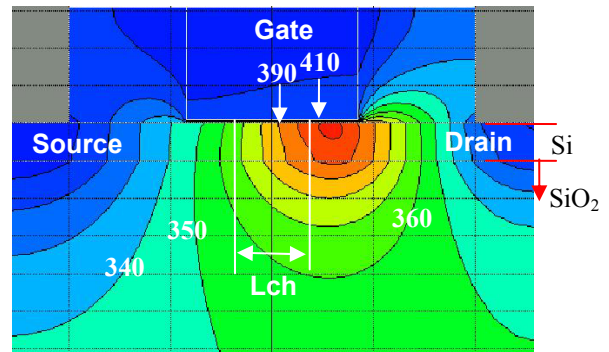
FIGURE 8: Two-dimensional contour plot of the acoustic phonon temperature. The interval between contours is 10 Kelvin. $V_{GS} = V_{DS} = 1$ V and $I_{DS} = $ ~0.4 mA/µm.
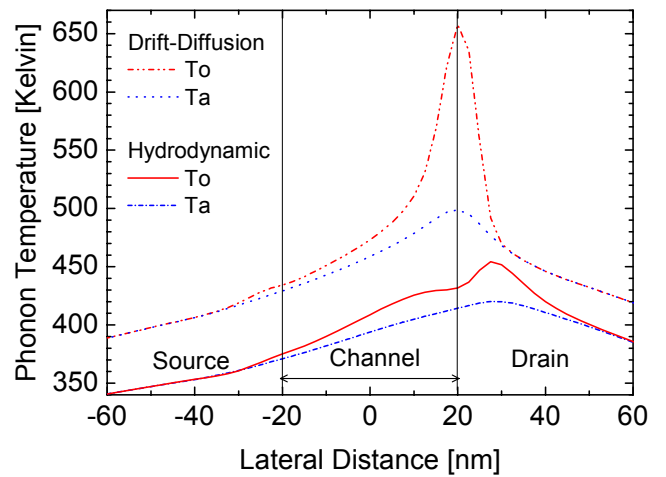
FIGURE 9: Comparison between the drift-diffusion models and hydrodynamic models. The heat generation in the drift-diffusion is implemented as $J \cdot E$.

Fig. 9 shows the comparison between the drift-diffusion

models and hydrodynamic models. In the drift-diffusion models, the heat generation is dominated by $J \cdot E$, while in the hydrodynamic models it is due to the electron-phonon collision term as expressed in Eq.4. The significant difference is the location where the temperature profile has its peak. While the peak temperature with the heat generation term of $J \cdot E$, is located at the edge of the channel (where E has its peak), the hydrodynamic model predicts that the peak temperature is shifted deep into the drain. The result from the hydrodynamic model is more physical, because electrons travel a few mean-free-paths after gaining energy in high electric field region, and then release the energy to the lattice inside the drain region. It should be also pointed out that the heat generation by $J \cdot E$ is also more severely localized, therefore the peak temperature of the hotspot is higher in the drift-diffusion simulation results. These discrepancies between the drift-diffusion and hydrodynamic models are also demonstrated and verified by Monte Carlo simulations [2].

IV. CONCLUSIONS

The optical and acoustic temperature systems are fully coupled to the hydrodynamic model. This system can capture most physical phenomena of the heat generation and conduction inside nanoscale devices. Due to the relatively long energy relaxation time between optical phonons and acoustic phonons, the optical phonon temperature is considerably raised so that the electrical characteristics are noticeably affected. The extracted temperature profiles show qualitatively good agreement with the already published Monte Carlo simulation results.

ACKNOWLEDGEMENT

REFERENCES

[1] E. Pop et al., "Detailed Heat Generation Simulations via the Monte Carlo Method," *Proceedings of SISPAD*, September, 2003, pp. 121-124.

[2] E. Pop, "Self-Heating and Scaling of Thin Body Transistors," *Ph.D. Dissertation*, Stanford University, December, 2004.

[3] E. Pop et al., "Thermal Phenomena in Nanoscale Transistors," *Int. Soc. Conf. Thermal Phenomena,* June, 2004. pp.1-7.

[4] M. Asheghi et al., "Thermal Conductivity Model for Thin Silicon-on-Insulator Layers at High Temperatures," *Int. SOI Conf.,* 2002, pp. 51-52.

[5] O. Tornblad et al., "Modeling and Simulation of Phonon Boundary Scattering in PDE-based Device Simulators," *Proceedings of SISPAD*, 2000, pp. 58-61.

[6] *PROPHET User Reference Guide*, MTAssociates, 2003.

[7] T. Oh, "AC and Noise Analysis of Deep-submicron MOSFETs," *Ph.D. dissertation*, Stanford University, February, 2004.

[8] J. Lai and A. Majumdar, "Concurrent Thermal and Electrical Modeling of Sub-micrometer Silicon Devices," *J. Appl. Phys.*, 79 (9), 1996, pp.7353-7361.

[9] D. A. Antoniadis et al., "MIT Well Tempered Bulk-Si NMOSFET Device," MIT, MS, 1999, http://www-mtl.mit.edu/Well

[10] D. Esseni et al., "Low Field Electron and Hole Mobility of SOI Transistors Fabricated on Ultrathin Silicon Films for Deep Submicrometer Technology Application," *IEEE Trans. on Electron Devices*, vol. 48, December 2001, pp. 2842-2850.

[11] K. Uchida et al., "Experimental Study on Carrier Transport Mechanism in Ultrathin-Body SOI N- and P-MOSFETs with SOI Thickness Less than 5nm," *IEDM Tech. Digest*, 2002, pp.47-50.